01,09

Modeling the motion of edge dislocations in aluminum under high shear strains using molecular dynamics

© I.S. Sugonyako[1], R.I. Babicheva[2,3], A.Yu. Morkina[1,3,4], D.V. Tarov[3,4], S.V. Dmitriev[1,2,4]

[1] Ufa State Petroleum Technological University,
Ufa, Russia
[2] Institute of Molecule and Crystal Physics,
Subdivision of the Ufa Federal Research Centre of the Russian Academy of Sciences,
Ufa, Russia
[3] Ufa University of Science and Technology,
Ufa, Russia
[4] Institute for Metal Superplasticity Problems, Russian Academy of Sciences,
Ufa, Bashkortostan, Russia

E-mail: sgnilya@mail.ru

Received August 4, 2025
Revised August 15, 2025
Accepted August 17, 2025

The molecular dynamics method is used to study the motion of a pair of edge dislocations of opposite signs in a single crystal of aluminum with an fcc lattice under different shear stresses and temperatures. The dimensions of the computational cell with periodic boundary conditions in all three directions are chosen so that the dislocations do not interact with each other. The range of sufficiently large shear stresses is studied, when the above-barrier slip of dislocations is realized and their velocity decreases with increasing temperature due to an increase in viscous friction. The stacking fault energy is calculated and the oscillation frequency of the dislocation line is estimated. The obtained results are consistent with the known results of modeling and experimental data, and can be used to interpret the electroplasticity effect.

Keywords: molecular dynamics, edge dislocation, shear stresses, aluminum, Peierls–Nabarro potential.

DOI: 10.61011/PSS.2025.08.62251.221-25

1. Introduction

For most metals, at the normal conditions the basic mechanism of plastic deformation is sliding and climbing of dislocations and only in materials with a nanocrystalline structure that have a dense grid of grain boundaries the deformation is mostly contributed by grain boundary sliding [1,2]. In recent decades, an electroplasticity effect (EPE) has gained interest [3–5], which was discovered by Troitskii in 1969 [6] and now various methods are proposed for its application [7–10]. A physical nature of the EPE is still actively discussed. In addition to an electron wind hypothesis [11], a hypothesis of dislocation heating by an electron flux is discussed [12–15], since they offer increased resistance to a current. After receiving thermal energy from the electron flux, dislocations have high mobility. It explains an increase of plasticity of the metal without significant heating of the metal on average, which is exactly determined as the EPE [16]. More detailed discussion of the above-described EPE mechanism requires information about how mobility of dislocations depends on the temperature and a stress-strain state of the metal. It is this problem that motivated this research.

It is known that dislocations in metals move as per two mechanisms: thermofluctuation mobility and dynamic overcoming of the Peierls–Nabarro barrier [17]. During thermoactivated motion, dislocations that are in a field of shear stresses, overcome the Peierls–Nabarro barrier due to thermal oscillations of atoms, by formation and motion of the kinks on the dislocations. A speed of dislocation movement with the increase of the temperature significantly increases in this case, since probability of kink origination on a dislocation line increases [18]. This mechanism is typical for slowly moving dislocations under effect of weak shear stresses. With dynamic or, in other words, over-barrier motion of the dislocations, the acting shear stress is sufficiently high to overcome the Peierls–Nabarro barrier without an additional contribution by thermofluctuation. In this case, the increase of the temperature results in a decrease of the dislocation speed, since they are subjected to increasing viscous deceleration. Dynamic deceleration is manifested not only for fast dislocations, but for slow ones as well to determine a rate of decay of oscillation motion of dislocation segments between obstacles and kinetics of thermofluctuation overcoming of potential barriers by the dislocations [19]. Therefore, it is important to study various ranges of the temperatures and the shear stresses to investigate motion of the dislocations.

It is difficult to experimentally study physical processes that occur in the metals during motion of the dislocations, since an experiment method is quite complicated, their application field is limited and they require costly

equipment [20]. Therefore, it is relevant to use computer simulation methods, namely, a molecular dynamics method (MD), for such studies. Molecular dynamics means numerical integration of equations of the classical Newtonian mechanics, which describe motion of separate atoms in a solid body or liquid using an interparticle interaction potential that takes into account properties of a studied substance [21]. Simulation by the MD method involves a wide use of potentials that are created by an embedded atom method (EAM potentials) and take into account not only interaction between the very atoms, but interaction between the atoms and an electron gas, thereby resulting in multiparticle interatomic interactions [22]. We should note a large progress in development of machine learning potentials (MLI potentials) [23–26], which significantly exceed the EAM potentials in accuracy, but are inferior to them in terms of speed by at least an order [27].

Due to a limited computer power, the MD simulation deals with small volumes of the substance. As known, the separate dislocations create long-range fields of elastic distortions of the lattice and then there is a problem of eliminating interaction of the dislocation in question with such fields created by other dislocations [28–32]. The aim of the present study was to investigate motion of the dislocations in an aluminum single crystal using periodic boundary conditions that make it possible to fully zero forces of interactions between the dislocations when correctly selecting sizes of a computational cell. The simulation was at various values of the shear stress and the temperature. Due to the above-mentioned limitedness of computers resources, we managed to consider only a case of over-barrier sliding of the dislocations with the shear stresses noticeably exceeding an aluminum's flow stress that is 45−55 MPa depending on a structure state. The studied temperature interval from 50 to 700 K covers ranges of cryogenic and hot deformation (the melting temperature of aluminum is 934 K). The electroplastic deformation usually takes place without significant heating of the metal on average, but around the dislocations the material is heated more strongly, therefore it is also interesting to simulate the dislocations at the higher temperatures.

2. Model

To simulate by the MD method, the LAMMPS software was used, while the OVITO software was used to visualize calculation results. In order to study dynamics of edge dislocations in aluminum, we constructed the computational cell of an FCC crystal with coordinate axes that were oriented according to the basic slip system $[110]$ $(\bar{1}1\bar{1})$ that was typical for the metals with the FCC lattice.

Presently, motion of the dislocations in aluminum is studied using models with various boundary conditions [11,19,21,33–36]. Unlike many existing studies, in which the periodic boundary conditions were pre-defined by one or two axes [19,21], in our model the periodic boundary

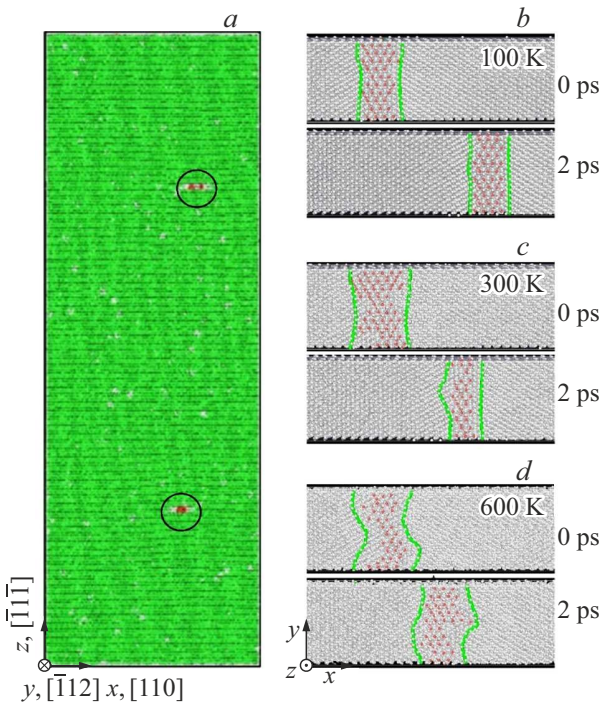

Figure 1. (a) Computational cell and the directions of the coordinate axes. The two split edge dislocations are encircled. (b–d) Motion of the dislocations in the sliding plane at the shear stress of 140 MPa at the times 0 and 2 ps at the temperature (b) 100 K, (c) 300 K and (d) 600 K. The lines of partial dislocations are shown in green, the atoms with HCP coordination are shown in red, they are arranged on stacking faults.

conditions were pre-defined by the three axes (x, y, z) in order to simulate motion of a pair of edge dislocations of opposite signs. When selecting the size of the lattice cell, we took into account that in order to provide minimum interaction between the upper and lower dislocations of opposite signs, a height of the lattice cell shall exceed its length at least in three times [37]. Here, we use a fact that fields of stresses from a chain of equidistant dislocations exponentially decrease with a distance. Thus, the sizes of the selected computational cell were $171.4 \times 24.7 \times 517.8$ Å. Figure 1, a shows the computational cell and directions of the axes. Figure 1, b–d shows oscillations of partial dislocations at the various temperatures. It is clear that the size of the computational cell along the axis x is sufficient to comprise several kinks on the dislocation line, which are well visible at the higher temperatures.

A length of the Burgers vector for the full dislocation is calculated by the formula

$$|\mathbf{b}| = \frac{a}{2}\,|\langle 110\rangle| = \frac{a}{\sqrt{2}}, \qquad (1)$$

where $a = 4.04$ Å is an equilibrium lattice parameter. Correspondingly, by substituting into (1), we obtain $|\mathbf{b}| = 2.8567$ Å.

For the molecular-dynamics simulation, we used the interparticle interaction potential presented in the study [38]. The simulation was at the temperatures $T = 50$, 100, 200, 300, 400, 500, 600, 700 K and shear strains

$$\varepsilon_{xz} = \frac{n|\mathbf{b}|}{L}, \tag{2}$$

where n — the natural number, L — the height of the lattice cell. Then, the respective shear stress is

$$\sigma_{xz} = G\varepsilon_{xz}, \tag{3}$$

where $G = 25.5$ GPa — the shear modulus of aluminum [39]. For $L = 517.8$ Å we considered the values $n = 1$, 2 and 4 and, besides, for the cell of the double height, $L = 1035.6$ Å, we considered the case when $n = 1$. Thus, the shear strains $\varepsilon_{xz} = 0.00275$, 0.0055, 0.011 and 0.022 were considered, to which the shear stresses $\sigma_{xz} = 70$, 140, 280 and 561 MPa corresponded. We note that these values are above the flow stress of pure aluminum, for which the values $\sigma_y = 30-55$ MPa are given depending on a grain size and a purity degree; therefore, motion of the dislocations in the performed calculations is over-barrier motion.

The simulation consisted of the following stages:

1. Creation of the ideal crystal FCC lattice of aluminum with the pre-defined sizes and crystal-lattice orientation with the periodic boundary conditions in the three dimensions.

2. Cutting out two adjacent atomic planes (110) of the common thickness $|\mathbf{b}|$ and height $L/2$ with subsequent energy minimization resulting in collapse of section edges and formation of the pair of the split edge dislocations of opposite signs. The minimization was carried out in an NVE assembly for 5 ps.

3. Holding for 1 ps in the NVE assembly for relaxation of internal stresses and for 10 ps in an NPT assembly at the temperature of a subsequent shear in order to transfer the system into an equilibrium state.

4. Application of homogeneous shear strain ε_{xz}.

5. Molecular-dynamics calculation for 10 ps after application of the shear with recording of dislocation motion.

We note importance of the stage 2, which includes splitting of the full dislocation that is energetically less favorable for this FCC lattice, into two partial edge dislocations as per the expression:

$$\frac{1}{2}a[110] = \frac{1}{6}a[21\bar{1}] + \frac{1}{6}a[121]. \tag{4}$$

The pair of the split dislocations occurred as a result of crystallite relaxation can be considered as a dislocation loop. Therefore, the upper and lower dislocations in Figure 1, *a* have an opposite topological charge and when the positive shear stress σ_{xz} is applied they will slide along the axis x in the opposite directions.

A stacking fault is formed between the partial dislocations. The split of the full dislocation is stable with a minimum of the energy of a system that consists of the two partial dislocations and the stacking fault binding them. At the same time, tensioning of the stacking fault tends to tighten up the partial dislocations together, overcoming a force of their repulsion. Consequently, a width of the splitting area of the partial dislocations is determined by the energy of the stacking fault: the smaller the energy of the stacking fault, the larger the distance between the partial dislocations [40].

The speed of the dislocations was determined as a sum of the distances transmitted by the two partial dislocations for a certain time period, which is divided by this time period. For the slower dislocations, we selected a longer time period in order to record the distance transmitted by them with sufficient accuracy. For the shear stresses 140, 280 and 561 MPa the calculation time was 2 ps at the temperatures 50, 100 and 200 K; it was 3 ps at the temperatures 300 and 400 K; it was 4 ps at the temperatures 500 and 600 K and it was 5 ps at the temperature of 700 K. For the double-height lattice, at the shear stress of 70 MPa, the calculation time was 4 ps for all the cases, since at this value of the stress the temperature slightly affected the speed of the dislocations.

In order to study oscillations of the partial dislocations due to thermofluctuations without effect of the shear, the calculations were performed for the temperatures 100, 300 and 600 K.

The simulation for determining the stacking fault energy (SFE) consisted of the following steps:

1. Creation of the ideal crystal FCC lattice of aluminum with the sizes $171.4 \times 24.7 \times 517.8$ Å.

2. Incorporation of the three parallel stacking faults into the system at the distance $5|\mathbf{b}|$ from each other by displacing respective atomic units by $|\mathbf{b}|/\sqrt{3}$ along the axis y, which is equivalent to displacement by $a/\sqrt{3}$ along the direction $\{112\}$ [41,42].

3. Energy minimization in the NVE assembly for 5 ps and holding at the temperature of 10 K for 10 ps in the NPT assembly.

4. Calculation of the SFE.

3. Results and discussion

3.1. Motion of dislocations

Figure 2 shows graphs of the dependence of the distance transmitted by the upper and lower partial dislocations on time at the shear stress of 280 MPa and the temperatures (*a*) 100 and (*b*) 500 K. It is clear that at the considered time portion the dislocations move approximately at the same speed, wherein the motion speed decreases with an increase of the temperature. The speed of the dislocations was determined within the portion of the linear dependence $x(t)$.

Figure 3 shows the dependences of the stress σ_{xz} on time and Figure 4 shows the dependences of other components of the stress tensor on time at the shear stress $\varepsilon_{xz} = 0.0055$ and at the various temperatures. It is clear from Figure 3

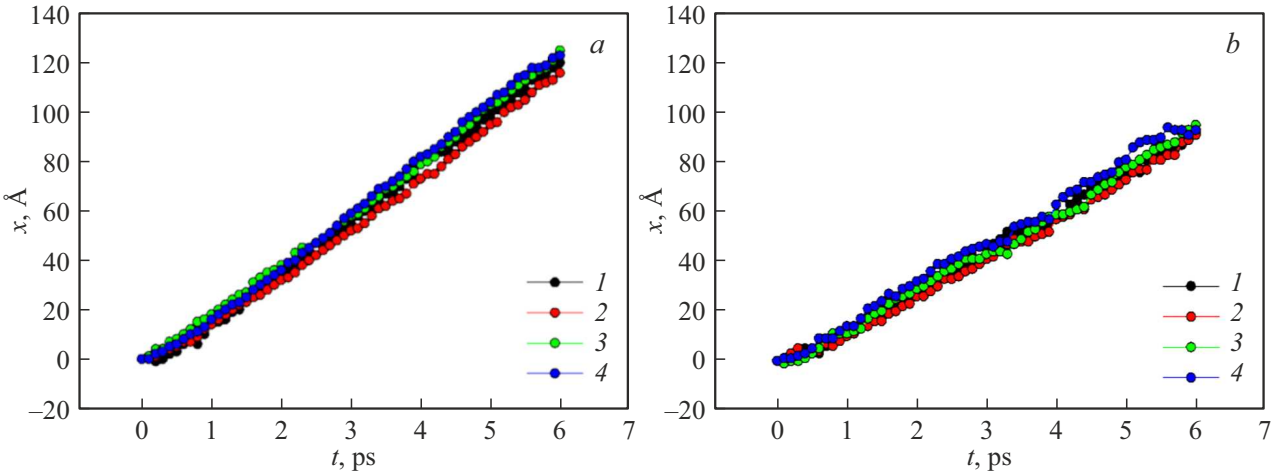

Figure 2. Dependence of the speed of the partial dislocations on time at the shear stress of 280 MPa at the temperature: *a* — 100, *b* — 500 K, where *1, 2* — the upper left and right partial dislocations, respectively, *3, 4* — the lower left and right partial dislocations, respectively.

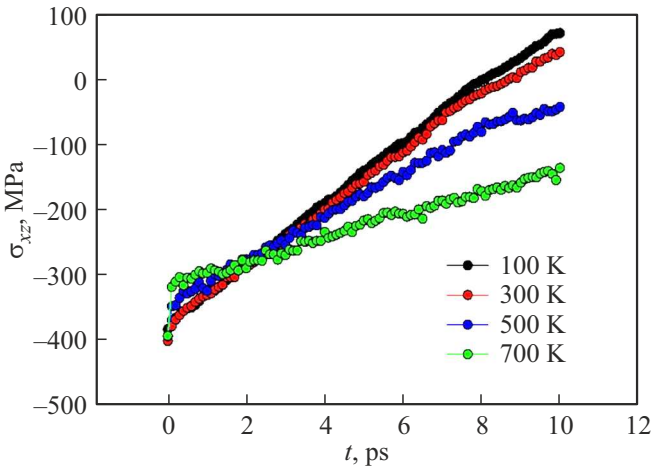

Figure 3. Dependence of the shear stress σ_{xz} on time with the shear strain $\varepsilon_{xz} = 0.0055$.

that the stress σ_{xz} tends to zero with time. Oscillating approximation of the shear stress to zero is observed at the low temperatures, so is relaxation approximation thereof at the high temperatures, which is related to the increase of viscosity of the material with the increase of the temperature. As can be seen from Figure 4, at all the temperatures the stresses σ_{xx}, σ_{yy}, σ_{zz}, σ_{xy}, σ_{yz} remain to be small as compared to the stress σ_{xz}.

Figure 5 shows graphs of the dependence of the speeds of the dislocations on the temperature at the various values of the shear strain, while Figure 6 shows graphs of the dependence of the stress σ_{xz} on the temperature in the same time interval, in which the speed of the dislocations was calculated.

It is clear from Figure 5 and Figure 6 that with the increase of the temperature the speed of motion of the dislocations and the stresses σ_{xz} decrease. At the same time, with the increase of the temperature the shear stresses σ_{xz} significantly decrease at the shear strain $\varepsilon_{xz} = 0.022$ and they less significantly decrease when $\varepsilon_{xz} = 0.011$ and are almost unchanged when $\varepsilon_{xz} = 0.0055$ and $\varepsilon_{xz} = 0.00275$. It is related to dynamic overcoming of the Peierls–Nabarro potential by the dislocations due to effect of the high shear stresses (which exceed a yield strength of this material, which is 55 MPa and 45 MPa in the initial and annealed states, respectively [43]) without significant contribution by thermofluctuation. Deceleration of the dislocations with the increase of the temperature is due to the increase of viscosity of medium, in which the dislocation moves.

It is assumed that at the lower shear stresses (below the yield strength) we enter an area of thermofluctuation mobility, where the speed of motion of the dislocations will increase with the increase of the temperature. At the same time, the dislocations will move much more slowly and their speed will be required to be measured at much longer time intervals.

3.2. Oscillation of dislocations

Figure 7 shows the images of the partial dislocations in a section in plan view at the zero shear stress and at the temperatures 100, 300 and 600 K. The images are provided with the interval of 0.4 ps. In all the cases, a period of oscillations of the dislocation line is about 0.1 ps. It is clear that with the increase of the temperature the amplitude of oscillations of the dislocations increases due to thermofluctuation of the atoms.

3.3. Stacking fault energy

The three stacking faults at the distance of $5|\mathbf{b}|$ were incorporated into the computational cell with the periodic

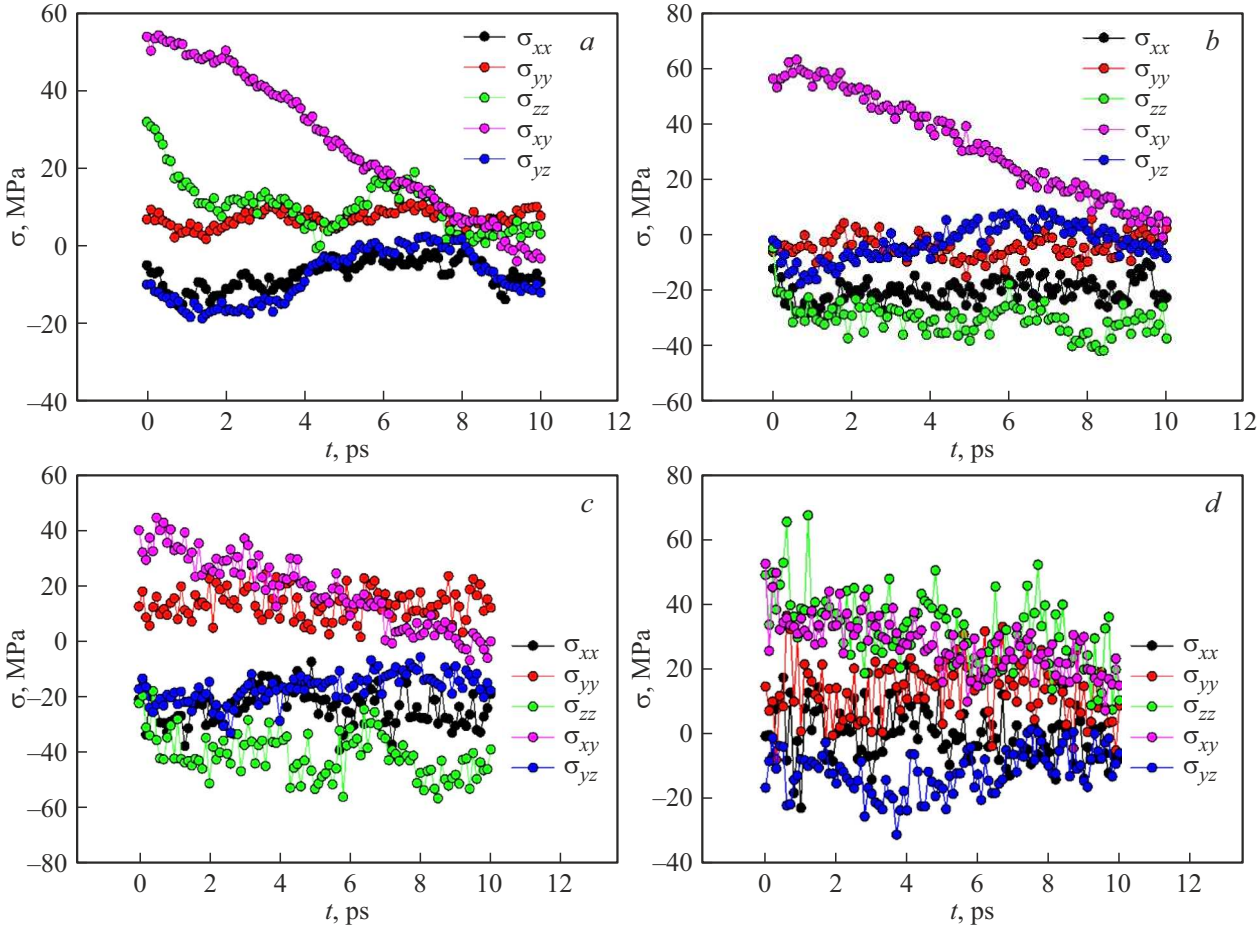

Figure 4. Dependence of various components of the stress tensor (except for σ_{xz}) on time with the shear strain $\varepsilon_{xz} = 0.0055$ and at the temperature: *a* — 100, *b* — 300, *c* — 500, *d* — 700 K.

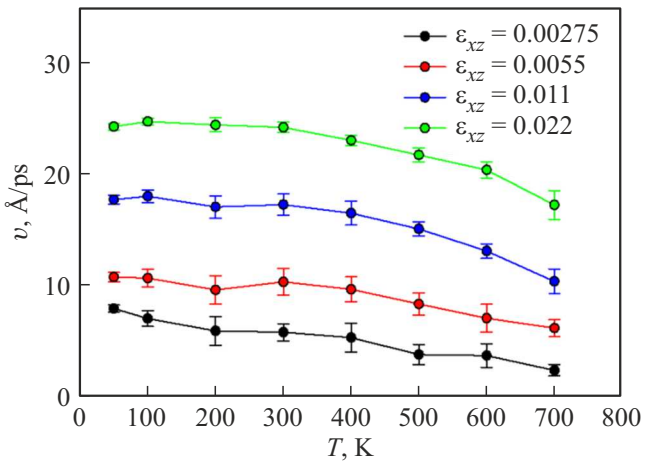

Figure 5. Dependences of the speed of the dislocations on the temperature at the various shear strains.

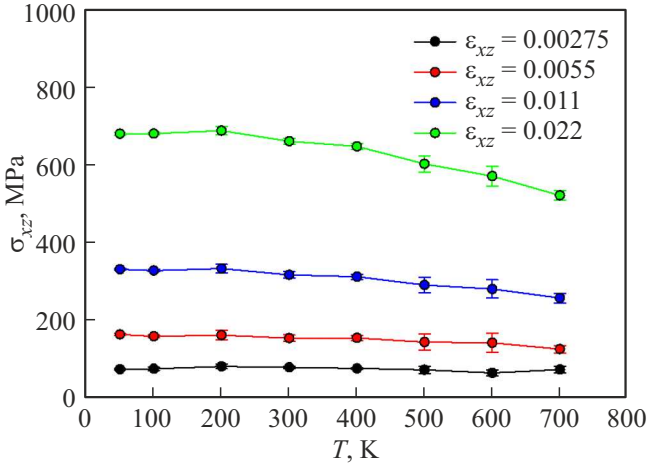

Figure 6. Dependences of the shear stresses σ_{xz} on the temperature within the interval, in which the speed of the dislocations was calculated.

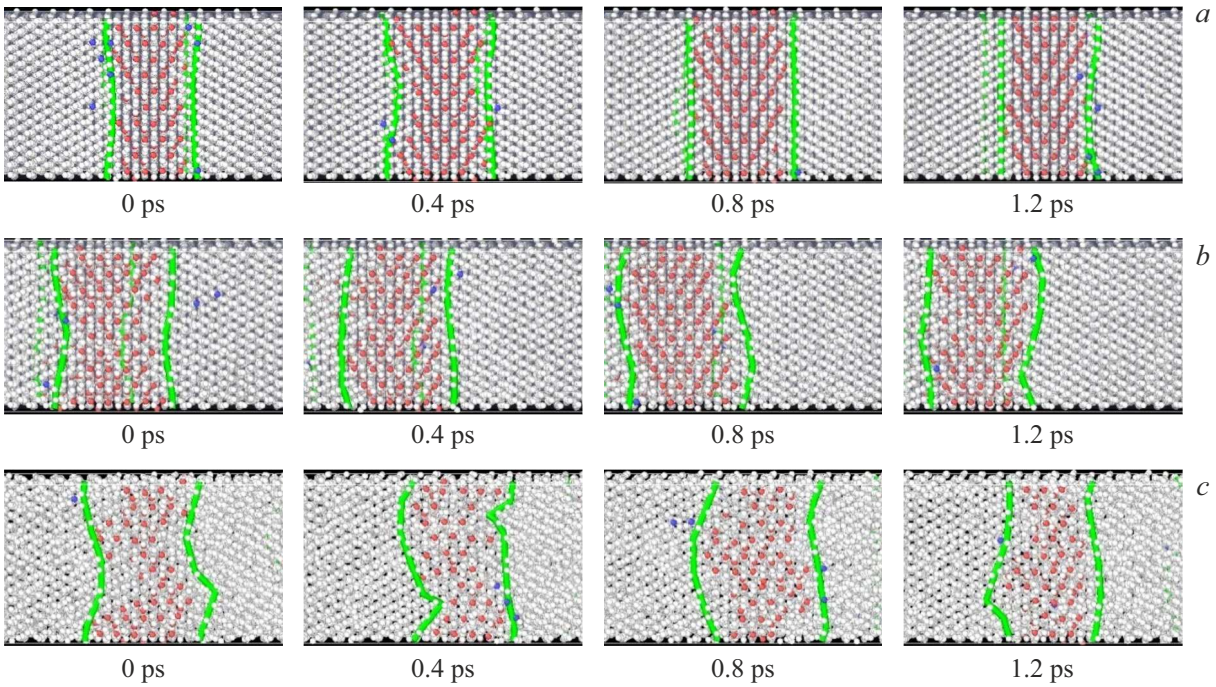

Figure 7. Image of the partial dislocations (the green lines) in a section in plan view at the zero shear stress at the temperatures: (*a*) 100, (*b*) 300, (*c*) 600 K. The dislocations for each temperature are shown in times with an interval of 0.4 ps.

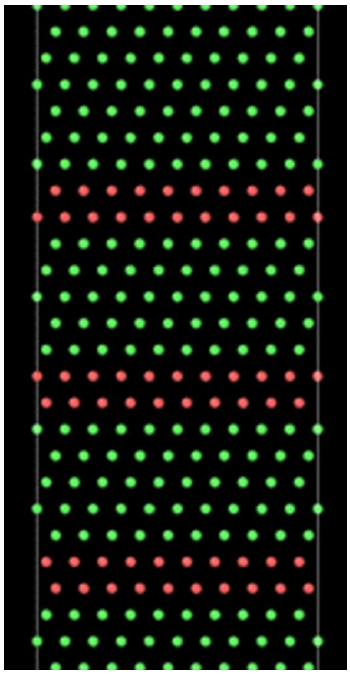

Figure 8. For the calculation of the stacking fault energy. The atoms with FCC (HCP) coordination are shown in green (red).

boundary conditions for SFE calculation, see Figure 8. The calculation was performed at the temperature of 10 K by the formula:

$$E_{SF} = \frac{E_2 - E_1}{3S}, \tag{5}$$

where E_1 — the potential energy of the ideal structure after minimization, E_2 — the structure defect energy after minimization, S — the area of one stacking fault. Using the numerical values $E_1 = -447380.34$ eV, $E_2 = -447275.41$ eV, $S = 4233.58$ Å^2, we find that

$$E_{SF} = 0.0082\,\text{eV/Å}^2 = 131\,\text{mJ/m}^2. \tag{6}$$

According to the literature data [44], the SFE value of aluminum is within the interval 80−150 mJ/m^2 and the obtained calculated value falls within this interval. Coincidence of the SFE with the experimental data indicates justifiability of selection of the used interatomic potential.

4. Conclusion

We have performed the molecular-dynamics simulation of motion of the edge dislocations in the FCC lattice of the aluminum single crystal at the various values of the shear stresses and the temperature. We have used the periodic boundary conditions with the pair of the edge dislocations of opposite sings in the computational cell, whereas only one dislocation was previously considered in many studies with using rigid boundary conditions along some directions [28,29,31]. Absence of interaction between the pair of the dislocations in the computational cell is achieved in the present study by selecting a cell size ratio based on the fact that the elastic fields created by the chain of the equidistant dislocations exponentially decrease with the distance from the chain.

The full dislocation was split into two partial dislocations, between which the stacking fault with the HCP structure was formed, which is typical for the FCC metals. The stacking fault energy is calculated. The obtained value $E_{SF} = 131\,\text{mJ/m}^2$ is within the range of the experimental data $80-150\,\text{mJ/m}^2$ [44], thereby indicating a good quality of the used interatomic potential.

Within the studied range of the shear stresses $70-561\,\text{MPa}$ (above the flow stress that is $30-55\,\text{MPa}$ [43]), the Peierls–Nabarro potential is dynamically overcome by the dislocations. As a result, the increase of viscous friction with the increase of the temperature determined reduction of the speed of the dislocations with the increase of the temperature, see Figure 5.

It is found when studying the process of oscillations of the lines of the partial dislocations at the various temperatures without applying the shear stress that the typical oscillation period is 0.1 ps. A typical current pulse applied in EPE-study has duration of 10^{-4} s, i. e. for the time of transmission of one pulse the dislocation has time to complete 10^9 oscillations.

Let us show that the represented results are useful when discussing the EPE nature. It is known that the density of the dislocations after annealing is $\rho \sim 10^{12}\,\text{m}^{-2}$ and can be up to $\rho \sim 10^{16}\,\text{m}^{-2}$ in the highly deformed metals [45,46]. When considering an array of the equidistant parallel straight dislocations with the density of the dislocations ρ, the distance between the nearest dislocations in it will be $D \sim 1/\sqrt{\rho}$. We obtain that $D \sim 10^4$ Å in the annealed state and $D \sim 10^2$ Å in the deformed metal. We note that our calculations used the cell with the sizes $171.4 \times 24.7 \times 517.8$ Å, in which the two dislocations are arranged. Thus, we simulated the density of the dislocations, which corresponded to the highly deformed state.

Joule heat released at the dislocation propagates further on due to thermal conductivity into defectless areas of the crystal. By solving a thermal conductivity problem, it can be found how the temperature of a dislocation nucleus varies in time by taking into account a Joule heat influx rate and a heat outflow rate due to thermal conductivity. When knowing the temperature of the dislocation and the dependence of the speed of the dislocation on the temperature, one can construct a theory of electroplastic deformation. This theory shall also take into account a change of the density of the dislocations during electroplastic deformation.

The presented results can be useful when discussing the experimental studies for electroplasticity of aluminum and aluminum alloys that are electrosimulatedly formed [47], twisted [48], cyclically twisted [49] and tensioned [50]. Of interest, are studies on the influence of the current on a friction coefficient of aluminum [51], a compression ratio of titanium [52] as well as on vibrations of a metal, which are induced by current pulses.

It is planned in the next studies to determine the dependence of the speed of the dislocations on the temperature at the low values of the shear stresses, when the Peierls–Nabarro potential is overcome in a thermofluctuation way and it is expected that the speed of the dislocation increases with the temperature. These calculations will require many more resources, since the calculation time significantly increases.

Acknowledgments

The study was carried out by employees of a department „Equipment and Technologies for Welding and Control“ and Reverse Engineering Center of Ufa State Petroleum Technological University. The study was carried out within the framework of a program „PRIORITET 2030“ from the Ministry of Science and Higher Education of the Russian Federation. The study by R.I. Babicheva was supported by the Ministry of Science and Higher Education of the Russian Federation within the framework of the state assignment of the Ufa University of Science and Technology (No. 075-03-2024-123/1) of the Youthful Research Laboratory „Metals and Alloys under Extreme Loads“.

Funding

The study was carried out by employees of a department „Equipment and Technologies for Welding and Control“ and Reverse Engineering Center of Ufa State Petroleum Technological University. The study was carried out within the framework of a program „PRIORITET 2030“ from the Ministry of Science and Higher Education of the Russian Federation.

Conflict of interest

The authors declare that they have no conflict of interest.

References

[1] R.Z. Valiev, N.A. Enikeev, M.Yu. Murashkin, V.U. Kazykhanov, X. Sauvage. Scripta Mater. **63**, *9*, 949 (2010).
[2] Y. Zhang, S. Jin, P.W. Trimby, X. Liao, M.Y. Murashkin, R.Z. Valiev, J. Liu, J.M. Cairney, S.P. Ringer, G. Sha. Acta Mater. **162**, 19 (2019).
[3] A.P. Sutton, T.N. Todorov. Phys. Rev. Mater. **5**, *11*, 113605 (2021).
[4] X. Li, Q. Zhu, Y. Hong, H. Zheng, J. Wang, J. Wang, Z. Zhang. Nat. Commun. **13**, *1*, 6503 (2022).
[5] M.-J. Kim, T.-A. Bui-Thi, S.-G. Kang, S.-T. Hong, H. Nam Han. Curr. Opin. Solid State Mater. Sci. **32**, 101190 (2024).
[6] O.A. Troitskii. JETP Letters **10**, 11 (1969).
[7] L. Qian, L. Zhan, B. Zhou, X. Zhang, S. Liu, Z. Lv. Mater. Sci. Eng. A **812**, 141144 (2021).
[8] C. Li, Z. Xu, L. Peng, X. Lai. Int. J. Mech. Sci. **218**, 107081 (2022).
[9] J. Lozares, N. Otegi, J. Trinidad, M. Barrenetxea, I. Aizpuru, P. Jimbert, J. Mendiguren. Mech. Mater. **198**, 105136 (2024).
[19] K.V. Kukudzhanov, G.R. Khalikova, E.A. Korznikova, A.V. Chentsov, S.V. Dmitriev. Mech. Solids **59**, *5*, 3223 (2024).

[11] X. Ren, Z. Wang. Comput. Mater. Sci. **253**, 113818 (2025).
[12] V.I. Dubinko, V.F. Klepikov. Bull. Russ. Acad. Sci. Phys. **72**, *9*, 1188 (2008).
[13] X. Li, A.M. Minor. Microsc. Microanal. **28**, *S1*, 1938 (2022).
[14] V.V. Stolyarov. J. Mach. Manuf. Reliab. **52**, *4*, 313 (2023).
[15] S.V. Dmitriev, A.Y. Morkina, D.V. Tarov, G.R. Khalikova, D.U. Abdullina, P.S. Tatarinov, V.P. Tatarinov, A.S. Semenov, O.B. Naimark, A.V. Khokhlov, V.V. Stolyarov. Spec. Mech. Eng. Oper. Res. **1**, 27 (2024).
[16] V. Stolyarov, A. Misochenko. Materials **16**, *18*, 6270 (2023).
[17] V.L. Indenbom, A.N. Orlov. V sb.: „Dinamika dislokatsii", Kh., Izd. FTINT AN USSR (1968). S. 3. (in Russian).
[18] V.I. Al'shits, V.L. Indenbom. UFN **115**, *1*, 3 (1975). (in Russian).
[19] A.Yu. Kuksin, A.V. Yanilkin. FTT **55**, *5*, 931 (2013). (in Russian).
[20] L.E. Popov, M.I. Slobodskoi, S.N. Kolupaeva. Izvestiya vuzov. Fizika **49**, *1*, 57 (2006). (in Russian).
[21] A.Yu. Kuksin, V.V. Stegailov, A.V. Yanilkin. Fiziko-khimicheskaya kinetika v gazovoi dinamike, **7**, 27 (2008). (in Russian).
[22] M.H. Müser, S.V. Sukhomlinov, L. Pastewka. Adv. Phys. X, **8**, 2093129 (2023).
[23] Y.-W. Zhang, V. Sorkin, Z.H. Aitken, A. Politano, J. Behler, A.P. Thompson, T.W. Ko, S.P. Ong, O. Chalykh, D. Korogod, E. Podryabinkin, A. Shapeev, J. Li, Y. Mishin, Z. Pei, X. Liu, J. Kim, Y. Park, S. Hwang, S. Han, K. Sheriff, Y. Cao, R. Freitas. Model. Simul. Mater. Sci. Eng. **33**, *2*, 023301 (2025).
[24] N. Rybin, I.S. Novikov, A. Shapeev. Phys. Chem. Chem. Phys. **27**, *10*, 5141 (2025).
[25] A.A. Kistanov, I.V. Kosarev, S.A. Shcherbinin, A.V. Shapeev, E.A. Korznikova, S.V. Dmitriev. Mater. Today Commun. **42**, 111437 (2025).
[26] D.S. Ryabov, I.V. Kosarev, D. Xiong, A.A. Kudreyko, S.V. Dmitriev. Comput. Mater. Contin. **82**, *3*, 3797 (2025).
[27] I.V. Kosarev, S.A. Shcherbinin, A.A. Kistanov, R.I. Babicheva, E.A. Korznikova, S.V. Dmitriev. Comput. Mater. Sci. **231**, 112597 (2024).
[28] A.V. Yanilkin, V.S. Krasnikov, A.Yu. Kuksin, A.E. Mayer. Int. J. Plast. **55**, 94 (2014).
[29] A.Y. Kuksin, A.V. Yanilkin. Phys. Solid State **55**, *5*, 1010 (2013).
[30] A.Y. Kuksin, A.V. Yanilkin. Mech. Solids **50**, *1*, 44 (2015).
[31] A.Yu. Kuksin, V.V. Stegaĭlov, A.V. Yanilkin. Dokl. Phys. **53**, *6*, 287 (2008).
[32] G.E. Norman, A.V. Yanilkin. Phys. Solid State **53**, *8*, 1614 (2011).
[33] Yu.N. Osetsky, D.J. Bacon. Model. Simul. Mater. Sci. Eng. **11**, 427 (2003).
[34] G.P. Purja Pun, Y. Mishin. Acta Mater. **57**, *18*, 5531 (2009).
[35] K.D. Manukhina, V.S. Krasnikov, D.S. Voronin, A.E. Mayer. Comput. Mater. Sci. **244**, 113269 (2024).
[36] V.S. Krasnikov, A.E. Mayer. Int. J. Plast. **119**, 21 (2019).
[37] A. Kazakov, R.I. Babicheva, A. Zinovev, D. Terentyev, K. Zhou, E.A. Korznikova, S.V. Dmitriev. Tungsten **6**, *3*, 633 (2024).
[38] X.-Y. Liu, F. Ercolessi, J.B. Adams. Model. Simul. Mater. Sci. Eng. **12**, 665 (2004).
[39] N.M. Belyaev. Soprotivlenie materialov. Nauka, M. (1965), 856 s. (in Russian).
[40] O.P. Maksimkin. Defekty upakovki, ikh energiya i vliyanie na svoistva obluchennykh metallov i splavov. Almaty (2010), 70 s. (in Russian).
[41] L. Zhang, L. Cheng, T. Kiet, X. Zhao, L.-Q. Pei, M. Guillaume. Chin. Phys. B **24**, *8*, 088106 (2015).
[42] J.A. Zimmerman, H. Gao, F.F. Abraham. Model. Simul. Mater. Sci. Eng. **8**, *2*, 103 (2000).
[43] A.Y. Morkina, D.V. Tarov, G.R. Khalikova, A.S. Semenov, P.S. Tatarinov, I.A. Yakushev, S.V. Dmitriev. Facta Univ., Ser. Mech. Eng. **22**, *4*, 615 (2024).
[44] B. Hammer, K. Jacobsen, V. Milman, M.C. Payne. J. Phys.: Condens. Matter **4**, 10453 (1999).
[45] M.J. Zehetbauer. In: Investigations and Applications of Serve Plastic Deformation / Edited by T.C. Lowe, R.Z. Valiev. Springer Netherlands, Dordrecht. (2000). P. 81–91.
[46] G. Kapoor, T. Kvackaj, A. Heczel, J. Bidulska, R. Kocisko, Z. Fogarassy, D. Simcak, J. Gubicza. Materials **13**, *10*, 2241 (2020).
[47] S. Dou, Z. Liu, Z. Li, H. Shi, K. Zhou, J. Xia. Metals, **15**, *2*, 117 (2025).
[48] D. Dobras, Z. Zimniak, M. Dziubek. Mater. Res. Proc. **41**, 1408 (2024).
[49] D. Dobras, K. Jaśkiewicz, M. Zwierzchowski. Mater. Res. Proc. 54, 1005 (2025).
[50] A.Y. Morkina, D.V. Tarov, I.A. Yakushev, P.S. Tatarinov, E.A. Korznikova, S.V. Dmitriev. Procedia Struct. Integr. **65**, 158 (2024).
[51] S. Dou, K. Zhou, H. Qian, H. Shi, J. Xia. J. Tribol. **147**, *4*, 044201 (2025).
[52] O.E. Korolkov, A.A. Misochenko, V.V. Stolyarov. Ind. Lab. Diagn. Mater. **90**, *12*, 65 (2024).
[53] O.B. Skvortsov, V.I. Stashenko. Inorganic Materials: Applied Research **16**, *1*, 42 (2025).

Translated by M.Shevelev